

Phase transitions and remnants of fractionalization at finite temperature in the triangular lattice quantum loop model

Xiaoxue Ran,¹ Sylvain Capponi,² Junchen Rong,^{3,4} Fabien Alet,² and Zi Yang Meng^{1,*}

¹*Department of Physics and HK Institute of Quantum Science & Technology,
The University of Hong Kong, Pokfulam Road, Hong Kong*

²*Laboratoire de Physique Théorique, Université de Toulouse, CNRS, UPS, France*

³*Institut des Hautes Études Scientifiques, 91440 Bures-sur-Yvette, France*

⁴*CPHT, CNRS, École Polytechnique, Institut Polytechnique de Paris, Palaiseau, France*

The quantum loop model (QLM), along with the quantum dimer model (QDM), are archetypal correlated systems with local constraints. With natural foundations in statistical mechanics, these models are of direct relevance to various important physical concepts and systems, such as topological order, lattice gauge theories, geometric frustrations, or more recently Rydberg quantum simulators. However, the effect of finite temperature fluctuations on these quantum constrained models has been barely explored. Here we study, via unbiased quantum Monte Carlo simulations and field theoretical analysis, the finite temperature phase diagram of the QLM on the triangular lattice. We discover that the vison plaquette (VP) crystal experiences a finite temperature continuous transition, which smoothly connects to the (2+1)d Cubic* quantum critical point separating the VP and \mathbb{Z}_2 quantum spin liquid phases. This finite temperature phase transition acquires a unique property of *thermal fractionalization*, in that, both the cubic order parameter – the plaquette loop resonance – and its constituent – the vison field – exhibit independent criticality signatures. This phase transition is connected to a 3-state Potts transition between the lattice nematic phase and the high-temperature disordered phase.

Introduction.— Quantum dimer/loop models (QDM/QLM) serve as quintessential statistical models to describe the low-energy properties of many-body systems with local constraints occurring in frustrated magnets [1–13] or cold atom experiments [6, 14–21]. Given that each site on the lattice can only be connected to one/two dimer/loop segments, QDM/QLM encompass a wide range of phenomena, including spinless and topological excitations in unconventional superconductors [22–25], and facilitate the detection of new phases and dynamic phenomena in frustrated systems [1, 26–29]. The mapping between the QDM/QLM and Rydberg atom arrays enables the observation of emergent phases in programmable quantum simulators [6, 7, 14, 20, 30–32].

Recent work [28] has identified a hidden vison plaquette (VP) phase in the ground state phase diagram of the QLM on the triangular lattice, located between a lattice nematic (LN) (topologically trivial) phase and a \mathbb{Z}_2 topological quantum spin liquid (QSL) phases identified in previous investigations [3, 4]. At odds with the LN where the C_3 lattice rotational symmetry-breaking can be identified from loop patterns, the VP phase is symmetric in the loop configurations but exhibits translational symmetry-breaking in the off-diagonal plaquette loop resonance term (the kinetic term in the QLM), and its hidden constituent – the fractionalized vison field. The quantum critical point (QCP), separating the VP and \mathbb{Z}_2 QSL was found to be of the (2+1)d Cubic* universality class [28, 29] whereas the quantum phase transition between the LN and VP phases is first order, as

understood from the histogram of the vison fields [28] that change from face-cubic to corner-cubic symmetry-breaking.

The interplay between quantum and thermal fluctuations in the vicinity of a QCP [33] can offer finite-temperature signatures and insights of quantum criticality [34–38]. While several investigations focused on zero-temperature ($T = 0$) phases of QLM/QDM [1–6, 8, 10, 11, 28, 29, 39–41], there is almost no work on their finite- T properties, with the only (to the best of our knowledge) exception of the investigation of the square lattice QDM phase diagram [12], exhibiting Kosterlitz-Thouless transition and high- T criticality intrinsically connected to the bipartiteness of the square lattice. The critical behavior on *non*-bipartite lattices remains to be explored at nonzero temperature, which is of particular interest as their ground-state phase diagram generically differs from their bipartite counterparts.

In this work, we investigate the finite temperature phase diagram of the QLM on the triangular lattice addressing large systems with the sweeping cluster quantum Monte Carlo (QMC) method [42, 43], combined with exact diagonalization and field-theoretical analysis. Our results are summarized in the phase diagram of Fig. 1. As the temperature is increased from the ground-state, we observe a 3-state Potts continuous phase transition between the LN phase and the disordered phase. More interestingly, we discover that the VP crystal experiences a finite temperature continuous transition, which smoothly connects to the (2+1)d Cubic* QCP separating the VP and QSL phases. This finite- T phase transition exhibits remnants of the fractionalization observed at the QCP in that, both the plaquette loop resonance (the cubic order parameter) and the vison fields (its constituent) exhibit

* zymeng@hku.hk

criticality with a symmetry structure corresponding to the rank-2 symmetric traceless tensor and rank-1 fundamental vector representations of the Cubic* criticality. Although strong finite-size effects do not allow to make definitive statements about the exponents of this VP-Disorder continuous transition, we discuss interesting possible scenarios. This "thermal fractionalization" transition connects to the 3-state Potts transition line above the LN phase, as well as a first-order phase transition line between the LN and VP phases at low T .

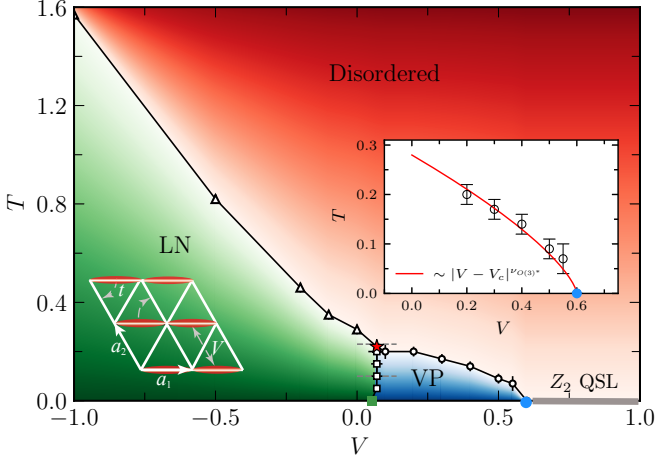


FIG. 1. Finite temperature (T) phase diagram of the QLM on the triangular lattice which exhibits different phases: Lattice Nematic (LN, green region), a Vison Plaquette (VP, blue region) phase, and a disordered phase (red) at high temperature. Additionally, the solid gray horizontal line marks the \mathbb{Z}_2 spin liquid phase only existing in the ground-state. The green ($V \simeq 0.05$) and blue ($V \simeq 0.6$) points correspond to the LN-VP and VP-QSL quantum phase transitions. The red star indicates a possible multicritical point at $(V, T) = (0.07(2), 0.22(2))$. The two dashed gray lines correspond to $T = 0.23$ (upper) and $T = 0.1$ (lower) used in Fig. 4. The inset zooms in at low- T near the VP-QSL Cubic* QCP, highlighting that the finite- T phase boundary scales as $T_c(V) \sim |V - V_c|^{\nu_{C^*}}$, with $\nu_{C^*} \simeq 0.7$ the correlation length exponent for the (2+1)d Cubic* universality class.

Model and Order Parameters.— The Hamiltonian of the QLM on a triangular lattice is defined as

$$H = -t \sum_{\alpha} (| \text{---} \text{---} \text{---} \rangle \langle \text{---} \text{---} \text{---} | + \text{h.c.}) + V \sum_{\alpha} (| \text{---} \text{---} \text{---} \rangle \langle \text{---} \text{---} \text{---} | + | \text{---} \text{---} \text{---} \rangle \langle \text{---} \text{---} \text{---} |), \quad (1)$$

where α denotes all the rhombi (with three orientations) on the triangular lattice. The local constraint of the fully packed QLM requires every site to be touched by two loop segments in any configuration. The kinetic term t generates plaquette loop resonance while respecting the local constraint, and V is the repulsion ($V > 0$) or attraction ($V < 0$) between loop segments on resonating plaquettes. $t = 1$ sets the energy scale and we perform QMC simulations for system sizes $N = L^2$ with

$L = 8, 12, 16, 20, 24, 28, 32$. Our exact diagonalization (ED) calculations are performed on a 28-sites cluster exhibiting a C_6 symmetry. On top of lattice symmetries, the model in Eq. (1) exhibits topological sectors labeled by the parity of the winding number of loops. For the QMC simulations, we work only in the $(0, 0)$ topological sector to decrease statistical errors, but we have checked using a fully-ergodic extension of the sweeping cluster algorithm [12] as well as ED data (see Supplemental Material (SM) [44]) that this does not affect our conclusions as the finite- T properties discussed in our work are dominated by the $(0, 0)$ sector. Further simulations details are provided in SM [44].

In the field theoretical description of the Cubic* VP-QSL QCP [28], the Lagrangian can be described using three scalars ϕ_i coupled together,

$$\mathcal{L}_{int} = m^2 (\sum_i \phi_i^2) + u (\sum_i \phi_i^2)^2 + \nu (\sum_i \phi_i^4) + \dots, \quad (2)$$

where the vison modes ϕ_i are defined as

$$\phi_i = \sum_{\mathbf{r}} (v_1(\mathbf{r}), v_2(\mathbf{r})) \cdot \mathbf{u}_i e^{i \mathbf{M}_i \cdot \mathbf{r}}, \quad i = 1, 2, 3, \quad (3)$$

with $\mathbf{M}_{i=1,2,3}$ the 3 \mathbf{M} points of the Brillouin zone and $v_{1,2}(\mathbf{r})$ the vison fields. The vector (ϕ_1, ϕ_2, ϕ_3) encapsulates the (2+1)d Cubic order parameters of the visons. The action was derived in Ref. [3] as possibly describing a LN-QSL direct QCP (not present in the triangular QLM). The VP phase was discovered and the Cubic* critical point was analyzed in later works using QMC simulation [28, 29], where the critical exponents were shown to agree with theoretical expectations via Monte Carlo simulations and conformal bootstrap [45–48]. The vison configuration is mapped from a loop configuration by setting a reference value $v_1(0, 0) = 1$ for the upper triangle of the first unit cell and computing $v_1(0, 0)v_{\gamma}(\mathbf{r}) = (-1)^{N_P}$, with N_P the number of loop segments intersected along a path P between triangles at $(0, 0)$ and \mathbf{r} . The mass term is identified as $m^2 \sim |V - V_c|$, and the phase transition occurs when $m^2 = 0$.

The order in the VP phase can also be identified from the static structure factor $C\mathcal{T}_{\mathbf{q}=\mathbf{M}}$ of the real space t -term correlator $\langle \mathcal{T}_i \mathcal{T}_j \rangle$.

$$C\mathcal{T}_{\mathbf{q}=\mathbf{M}} = \frac{1}{3N} \sum_{l=1}^3 \sum_{j=1}^N \sum_{k=1}^N e^{-i \mathbf{M}_l (R_j - R_k)} \langle \mathcal{T}_j \mathcal{T}_k \rangle. \quad (4)$$

Here $\mathcal{T}_j = t_{1,j} + t_{2,j} + t_{3,j}$ denotes the sum of the kinetic t -terms in H over the three rhombi centered around rhombus (or plaquette) j . In the symmetry description of the Cubic* criticality [28, 29], the kinetic terms ($t_1 = \phi_1 \phi_2, t_2 = \phi_2 \phi_3, t_3 = -\phi_1 \phi_3$) form the rank-2 symmetric traceless tensor representation of the Cubic group, while the vison modes (ϕ_1, ϕ_2, ϕ_3) form the rank-1 fundamental vector representation. To detect criticality, it is useful to consider the correlation ratio of \mathcal{T} defined

as $R_{CT} = 1 - C\mathcal{T}_{\mathbf{q}'}/C\mathcal{T}_{\mathbf{q}=\mathbf{M}}$, where $C\mathcal{T}_{\mathbf{q}'}$ is the average structure factor at the eight momenta $1/L$ away from \mathbf{M} .

Finally, the rotational symmetry breaking order parameter for the LN phase can be defined as $\langle D \rangle = \frac{1}{3L^2} \sum_c (|N_{\nearrow}^c - N_{\searrow}^c| + |N_{\nwarrow}^c - N_{\swarrow}^c| + |N_{\nearrow}^c - N_{\swarrow}^c|)$, where N_{\nearrow}^c , N_{\searrow}^c , and N_{\swarrow}^c count loop segments in configuration c for the three distinct orientations. Based on these considerations and order parameters, we now discuss the finite-temperature transitions out of the LN and VP phases.

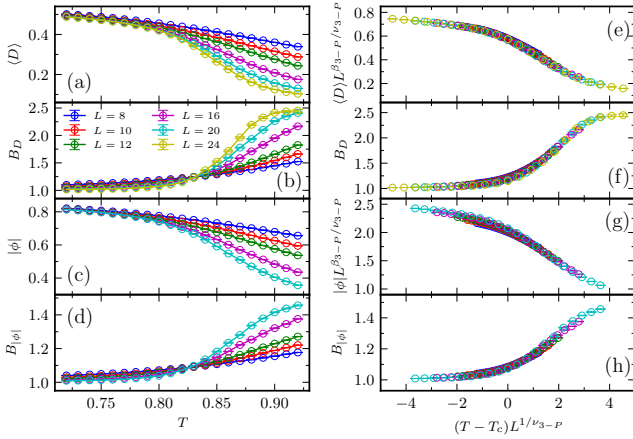


FIG. 2. Left panels present (a) the rotational symmetry breaking order parameter $\langle D \rangle$, (b) its Binder ratio B_D , (c) the vison parameter ϕ and (d) its Binder ratio $B_{|\phi|}$ for system sizes ranging from $L = 8$ to $L = 24$. Simulations are performed at $V = -0.5$, where the ground state is deep within the LN phase. The crossings in panels (b) and (d) indicate a phase transition occurring at $T_c = 0.82(2)$. The right panels display data collapse for $\langle D \rangle$, B_D , ϕ and $B_{|\phi|}$ using the critical exponents of the 3-state Potts model, where $\beta_{3P} = \frac{1}{9}$ and $\nu_{3P} = \frac{5}{6}$. The other finite- T LN transition points in Fig. 1 are determined similarly.

LN-Disorder 3-State Potts Transition.— First, we present the finite- T dependence of the nematic order parameter $\langle D \rangle$ and its Binder ratio $B_D = \langle D^4 \rangle / \langle D^2 \rangle^2$ in Fig. 2 (a) and (b) for $V = -0.5$ for various system sizes. The Binder ratio curves for different system sizes intersect at the transition temperature $T_c = 0.82(2)$. Additionally, we obtained a very good data collapse for $\langle D \rangle$ and B_D using the critical exponents of the 3-state Potts universality class, i.e. $\beta_{3P} = \frac{1}{9}$ and $\nu_{3P} = \frac{5}{6}$ [49, 50] in Fig. 2 (e) and (f). The three possible orientations of loops in the LN phase correspond to the three states of the Potts model [49–51]. The LN-Disorder transition points, denoted by empty triangles in Fig. 1, are determined with a similar analysis at other values of V .

In addition to the nematic order parameter, we further monitor the critical behavior of ϕ , defined in Eq. (3), for the LN-Disorder transition. The $|\phi|$ and its Binder ratio $B_{|\phi|} = \langle |\phi|^4 \rangle / \langle |\phi|^2 \rangle^2$ at $V = -0.5$ are shown in Fig. 2 (c) and (d). Interestingly, a data collapse in Fig. 2 (g) and (h) can be obtained using the same exponents as for the nematic order parameter. This can be intuitively under-

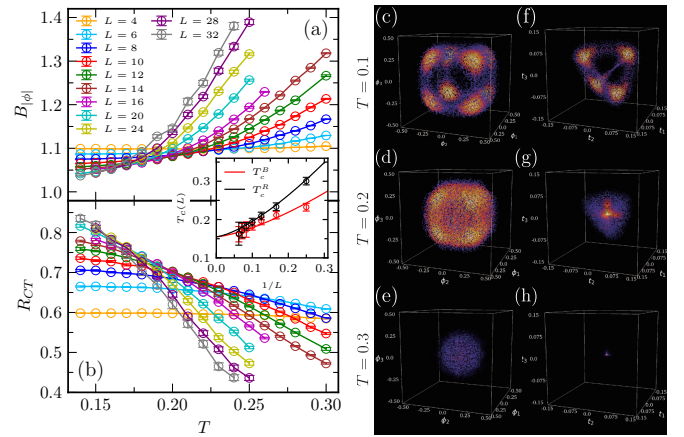


FIG. 3. (a) Binder ratio $B_{|\phi|}$ of the vison order parameter and correlation ratio R_{CT} of the t -terms for system sizes $L = 4$ to $L = 32$ for $V = 0.3$ (where the ground state is located within the VP phase). The inset illustrates the crossing between system sizes L and $2L$ for both $B_{|\phi|}$ and R_{CT} . Lines are fits to the form $T_c(L) = T_c(\infty) + aL^{-(\omega+1/\nu)}$, where ω is the correction exponent and ν the correlation length critical exponent. For $V = 0.3$, we obtain $T_c(\infty) = 0.16(1)$ and $\omega + 1/\nu = 1.5(1)$. Similar analysis for other V values are presented in SM [44]. The right panels display histograms for (ϕ_1, ϕ_2, ϕ_3) (left column) and $(t_1 = \phi_1\phi_2, t_2 = \phi_2\phi_3, t_3 = -\phi_1\phi_3)$ (right column) in a three-dimensional space within the VP phase ($T = 0.1$), near the transition point ($T = 0.2$), and in the disordered phase ($T = 0.3$). The system size is $L = 24$. These histograms illustrate the phase transition process, where the corner-cubic order in the VP phase, the cube in (ϕ_1, ϕ_2, ϕ_3) and tetrahedron shapes in (t_1, t_2, t_3) , shrink to a point in the disordered phase.

stood as the existence of a symmetry-breaking pattern in the loop configurations (leading to a finite expectation value for $\langle D \rangle$) inducing in a deterministic fashion a similar symmetry-breaking for the ϕ field (see Fig. 1 (b) in Ref. [28] for a schematic presentation of ϕ and loop-segment fields), with both 3-fold rotation and translation symmetry-breaking as in Eq. (3). Therefore D or ϕ fields can serve as similar order parameters for the LN-Disorder transition, and there is no “finite- T fractionalization” in this part of the phase diagram.

VP-Disorder Transition and “Finite-T Fractionalization”.— The transition out of the intrinsically quantum VP phase is more subtle as it cannot be easily captured by a classical constrained model with the same symmetries (e.g. a classical loop model would capture the LN-disorder phase transition, similar to how a classical dimer model captures the finite- T columnar phase transition in the square lattice QDM [12]). We first discuss theoretical expectations for the VP-Disorder transition before comparing to numerical simulations.

We consider finite- T fluctuations near the VP QCP at $V_c \simeq 0.6$ for Eq. (2), where the VP phase corresponds to the corner-cubic phase of the field theory. At finite T , the critical temperature should follow the power law behavior $T_c \sim |V - V_c|^{\nu_{C^*}}$, where ν_{C^*} is the critical exponents of

the Cubic* QCP (for more details see SM [44]).

The finite temperature VP-Disorder transition has two possible interpretations. Putting Eq. (2) at finite T , we expect a scalar theory respecting the Cubic symmetry in two spatial dimensions. One candidate theory is three decoupled copies of Ising models. Away from the quantum critical point, however, another candidate is the 4-state Potts universality class. In this case, the gauge invariant order parameter for the VP phase is given by the kinetic t_i -terms, which becomes the order parameter of the 4-state Potts model. The details of the above discussion are explained in SM [44]. The crucial difference between these two interpretations are whether the kinetic t_i -terms and the vison field ϕ will have different scaling dimensions at criticality.

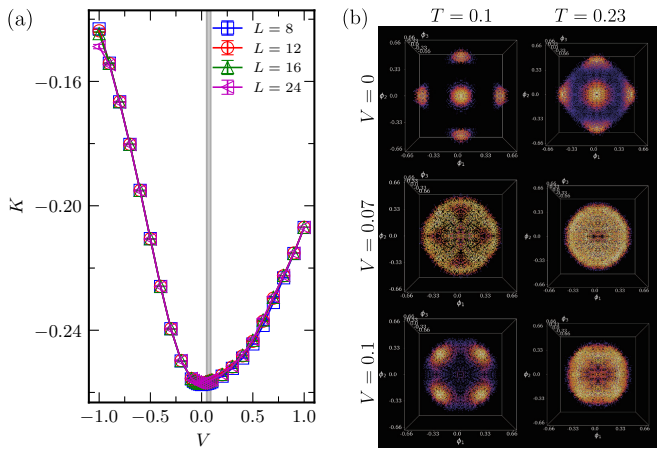


FIG. 4. (a) Kinetic energy density for $L = 8$ to $L = 24$ as a function of V at $T = 0.1$. The vertical line indicates the transition point at $V = 0.07(2)$. (b) Histograms of ϕ at $T = 0.1$ and $T = 0.23$ (dashed gray lines in Fig. 1) for a $L = 24$ system, with three rows corresponding to $V = 0$, $V = 0.07$, $V = 0.1$. The change in the slope of the K and the coexisting phases observed in the histogram at $V = 0.07$ suggest a first-order transition. The disappearance of the VP phase at all values of V as the temperature increases to 0.23 suggests the LN phase directly transitions to a disordered phase.

We now present numerical results for the VP-Disorder transition. Here we follow both kinetic \mathcal{T} -term and vison field ϕ to determine the transition temperature. Fig. 3 (c) - (h) are the histograms of the ϕ and \mathcal{T} order parameters across the VP-Disorder transition. In the VP phase, the three ϕ_i take values in the eight vertices of a cube while the scalar bilinear triplets, $\{\phi_1\phi_2, \phi_2\phi_3, -\phi_1\phi_3\}$ take four different values, forming a tetrahedron, see Fig. 3 (f). Fig. 3 (a), (b) depict the Binder ratio of $B_{|\phi|}$ and the correlation ratio of $R_{C\mathcal{T}}$ at $V = 0.3$ (in the middle of the VP phase) as a function of T for system sizes L up to 32. Both quantities exhibit crossings at finite T – a signature of a continuous VP-Disorder transition, albeit with obvious drifts of the crossing point as a function of L . Performing a crossing point analysis [52, 53] allows to determine the transition temperature in the thermody-

namic limit (see inset of the left panels of Fig. 3), as well as critical exponents. It is interesting that both quantities give rise to the same $T_c(\infty) = 0.16(1)$ (the T_c at other V values and the corresponding exponents are listed in the SM [44]). While resulting in consistent determinations of T_c (open circles in Fig. 1), the data analysis in the SM suggests that the critical exponents do not take a constant value along the thermal VP-disorder phase transition, and moreover that the estimated exponents are quite far off the candidate universality classes. We cannot exclude that this is due to the limited sample sizes simulated, and that on larger length scales, the exponents crossover –possibly slowly due to log corrections– to those e.g. of the 4-state Potts or decoupled Ising universality class, see [44].

It is also possible that finite-size estimates are affected by the proximity to the QCP or to a possible multicritical point where LN, VP and disordered phases meet (the red star in Fig. 1). Even though we can not determine the critical exponents accurately, it is quite remarkable that the ϕ and \mathcal{T} -terms appear to have different exponents, a situation quite different from the LN-Disorder transition but mimicking the QCP Cubic* behavior [28]. This could be interpreted in favor of the decoupled Ising scenario, instead of the 4-state Potts one. We furthermore plot the finite- T phase boundary $T_c(V)$ of the VP phase in the inset of Fig. 1, and found it follows nicely a functional form of $T_c(V) \sim |V - V_c|^{\nu_{C^*}}$, where $V_c = 0.6$ and $\nu_{C^*} \simeq 0.7$ [29]. Taken together, these two facts suggest that the VP-Disorder thermal transition is partially controlled by the Cubic* QCP at finite T , at least in its vicinity and on the finite sizes accessible to us.

LN-VP Transition and Multicritical point.— The LN-VP transition at $T = 0$ was identified to be first order, based on the phase coexistence in the ϕ histograms [28]. We repeat this analysis at finite T and display the corresponding ϕ histograms for the $L = 24$ system for $T = 0.1$ and $T = 0.23$ in panel (b) of Fig. 4. A coexistence of peaks located on face centers (for LN) and corners (for VP) of the cubes indicates a first-order phase transition at $V = 0.07$, which is further confirmed by the observed change in the slope of the kinetic energy density $K = \frac{1}{N} \sum_j \langle T_j \rangle$ in Fig. 4(a). The LN-VP phase boundary is found to be an approximately vertical line, indicated by white squares in Fig. 1. The VP phase vanishes around $T = 0.23$, as shown in the lower right corner of Fig. 4 (b). This behavior suggests the existence of a multicritical point at $(V, T) = (0.07(2), 0.22(2))$ marked by a red star in Fig. 1. More details are provided in the SM [44].

Discussion.— In this work, we obtained the finite temperature phase diagram of a non-bipartite constrained quantum many-body lattice model, the triangular lattice QLM, via unbiased large-scale QMC, assisted with ED and field-theoretical approaches. Importantly, we discovered that the VP crystal experiences a finite temperature continuous transition, with signatures of *thermal fractionalization*, in that, both the cubic order parameter (the plaquette loop resonance) and its constituent (the vi-

son field) exhibit critical behavior with symmetry structure corresponding to the rank-2 symmetric traceless tensor and rank-1 fundamental vector representations of the Cubic* criticality. This structure is maintained inside the entire VP phase, and the finite- T transition smoothly connects to the (2+1)d Cubic* QCP separating the VP and \mathbb{Z}_2 QSL phases, and to a 3-state Potts transition above the LN phase via a multicritical point. It will be interesting to investigate such thermal fractionalization in other constrained lattice models. Our results provide strong motivations to look for such phenomena in experiments on Rydberg atom quantum simulators or other synthetic platforms.

Acknowledgments.— We acknowledge discussions with Zheng Yan, Bhupen Dabholkar, and Yang Qi. X.R.R. and Z.Y.M. acknowledge the support from the Research Grants Council (RGC) of Hong Kong (Project Nos. AoE/P701/20, 17309822, C7037-22GF, 17302223), the

ANR/RGC Joint Research Scheme sponsored by RGC of Hong Kong (Project No. A_HKU703/22) and French National Research Agency (grant ANR-22-CE30-0042-01) and the HKU Seed Funding for Strategic Interdisciplinary Research. J.R. acknowledges the funding from the Simons programme général (2022-2031) in Institut des Hautes Études Scientifiques. J.R. also acknowledges funding from the European Union (ERC “QFTinAdS”, project number 101087025). Views and opinions expressed are however those of the authors only and do not necessarily reflect those of the European Union or the European Research Council Executive Agency. Neither the European Union nor the granting authority can be held responsible for them. We thank HPC2021 system under the Information Technology Services, University of Hong Kong, CALMIP (grant 2024-P0677), GENCI (project A0150500225) as well as the Beijing PARATERA Tech CO.,Ltd. (URL: <https://cloud.paratera.com>) for providing HPC resources that have contributed to the research results reported within this paper.

[1] R. Moessner and S. L. Sondhi, Resonating Valence Bond Phase in the Triangular Lattice Quantum Dimer Model, *Phys. Rev. Lett.* **86**, 1881 (2001).

[2] R. Moessner, S. L. Sondhi, and E. Fradkin, Short-ranged resonating valence bond physics, quantum dimer models, and Ising gauge theories, *Phys. Rev. B* **65**, 024504 (2001).

[3] K. Roychowdhury, S. Bhattacharjee, and F. Pollmann, Z_2 topological liquid of hard-core bosons on a kagome lattice at 1/3 filling, *Phys. Rev. B* **92**, 075141 (2015).

[4] X. Plat, F. Alet, S. Capponi, and K. Totsuka, Magnetization plateaus of an easy-axis kagome antiferromagnet with extended interactions, *Phys. Rev. B* **92**, 174402 (2015).

[5] Z. Yan, Y.-C. Wang, N. Ma, Y. Qi, and Z. Y. Meng, Topological phase transition and single/multi anyon dynamics of Z_2 spin liquid, *npj Quantum Mater.* **6**, 39 (2021).

[6] Z. Yan, R. Samajdar, Y.-C. Wang, S. Sachdev, and Z. Y. Meng, Triangular lattice quantum dimer model with variable dimer density, *Nat. Commun.* **13**, 5799 (2022).

[7] Z. Yan, Y.-C. Wang, R. Samajdar, S. Sachdev, and Z. Y. Meng, Emergent Glassy Behavior in a Kagome Rydberg Atom Array, *Phys. Rev. Lett.* **130**, 206501 (2023).

[8] R. Moessner, S. L. Sondhi, and P. Chandra, Phase diagram of the hexagonal lattice quantum dimer model, *Phys. Rev. B* **64**, 144416 (2001).

[9] D. A. Ivanov, Vortexlike elementary excitations in the Rokhsar-Kivelson dimer model on the triangular lattice, *Phys. Rev. B* **70**, 094430 (2004).

[10] A. Ralko, M. Ferrero, F. Becca, D. Ivanov, and F. Mila, Zero-temperature properties of the quantum dimer model on the triangular lattice, *Phys. Rev. B* **71**, 224109 (2005).

[11] G. Misguich and F. Mila, Quantum dimer model on the triangular lattice: Semiclassical and variational approaches to vison dispersion and condensation, *Phys. Rev. B* **77**, 134421 (2008).

[12] B. Dabholkar, G. J. Sreejith, and F. Alet, Reentrance effect in the high-temperature critical phase of the quantum dimer model on the square lattice, *Phys. Rev. B* **106**, 205121 (2022).

[13] X. Ran, Z. Yan, Y.-C. Wang, J. Rong, Y. Qi, and Z. Y. Meng, Fully packed quantum loop model on the square lattice: Phase diagram and application for Rydberg atoms, *Phys. Rev. B* **107**, 125134 (2023).

[14] H. Bernien, S. Schwartz, A. Keesling, H. Levine, A. Omran, H. Pichler, S. Choi, A. S. Zibrov, M. Endres, M. Greiner, V. Vuletić, and M. D. Lukin, Probing many-body dynamics on a 51-atom quantum simulator, *Nature* **551**, 579 (2017).

[15] A. Keesling, A. Omran, H. Levine, H. Bernien, H. Pichler, S. Choi, R. Samajdar, S. Schwartz, P. Silvi, S. Sachdev, P. Zoller, M. Endres, M. Greiner, V. Vuletić, and M. D. Lukin, Quantum Kibble–Zurek mechanism and critical dynamics on a programmable Rydberg simulator, *Nature* **568**, 207 (2019).

[16] R. Samajdar, W. W. Ho, H. Pichler, M. D. Lukin, and S. Sachdev, Complex Density Wave Orders and Quantum Phase Transitions in a Model of Square-Lattice Rydberg Atom Arrays, *Phys. Rev. Lett.* **124**, 103601 (2020).

[17] S. Ebadi, T. T. Wang, H. Levine, A. Keesling, G. Semeghini, A. Omran, D. Bluvstein, R. Samajdar, H. Pichler, W. W. Ho, S. Choi, S. Sachdev, M. Greiner, V. Vuletić, and M. D. Lukin, Quantum phases of matter on a 256-atom programmable quantum simulator, *Nature* **595**, 227 (2021).

[18] P. Scholl, M. Schuler, H. J. Williams, A. A. Eberharter, D. Barredo, K.-N. Schymik, V. Lienhard, L.-P. Henry, T. C. Lang, T. Lahaye, *et al.*, Quantum simulation of 2D antiferromagnets with hundreds of Rydberg atoms, *Nature* **595**, 233 (2021).

[19] M. Kalinowski, R. Samajdar, R. G. Melko, M. D. Lukin, S. Sachdev, and S. Choi, Bulk and boundary quantum phase transitions in a square Rydberg atom array, *Phys. Rev. B* **105**, 174417 (2022).

[20] R. Samajdar, W. W. Ho, H. Pichler, M. D. Lukin, and S. Sachdev, Quantum phases of Rydberg atoms on a

kagome lattice, *Proc. Nat. Acad. Sci.* **118**, e2015785118 (2021).

[21] R. Verresen, M. D. Lukin, and A. Vishwanath, Prediction of Toric Code Topological Order from Rydberg Blockade, *Phys. Rev. X* **11**, 031005 (2021).

[22] S. A. Kivelson, D. S. Rokhsar, and J. P. Sethna, Topology of the resonating valence-bond state: Solitons and high- T_c superconductivity, *Phys. Rev. B* **35**, 8865 (1987).

[23] D. S. Rokhsar and S. A. Kivelson, Superconductivity and the Quantum Hard-Core Dimer Gas, *Phys. Rev. Lett.* **61**, 2376 (1988).

[24] G. Baskaran and P. W. Anderson, Gauge theory of high-temperature superconductors and strongly correlated Fermi systems, *Phys. Rev. B* **37**, 580 (1988).

[25] S. Sachdev and M. Vojta, Translational symmetry breaking in two-dimensional antiferromagnets and superconductors, [arXiv:cond-mat/9910231](https://arxiv.org/abs/cond-mat/9910231).

[26] R. Moessner, S. L. Sondhi, and P. Chandra, Two-Dimensional Periodic Frustrated Ising Models in a Transverse Field, *Phys. Rev. Lett.* **84**, 4457 (2000).

[27] Y. Jiang and T. Emig, String Picture for a Model of Frustrated Quantum Magnets and Dimers, *Phys. Rev. Lett.* **94**, 110604 (2005).

[28] X. Ran, Z. Yan, Y.-C. Wang, R. Samajdar, J. Rong, S. Sachdev, Y. Qi, and Z. Y. Meng, Hidden orders and phase transitions for the fully packed quantum loop model on the triangular lattice, *Communications Physics* **7**, 207 (2024).

[29] X. Ran, Z. Yan, Y.-C. Wang, J. Rong, Y. Qi, and Z. Y. Meng, Cubic* criticality emerging from a quantum loop model on triangular lattice, *Phys. Rev. B* **109**, L241109 (2024).

[30] G. Semeghini, H. Levine, A. Keesling, S. Ebadi, T. T. Wang, D. Bluvstein, R. Verresen, H. Pichler, M. Kalinowski, R. Samajdar, A. Omran, S. Sachdev, A. Vishwanath, M. Greiner, V. Vuletić, and M. D. Lukin, Probing topological spin liquids on a programmable quantum simulator, *Science* **374**, 1242 (2021).

[31] G. Giudici, M. D. Lukin, and H. Pichler, Dynamical Preparation of Quantum Spin Liquids in Rydberg Atom Arrays, *Phys. Rev. Lett.* **129**, 090401 (2022).

[32] Z. Zhou, Z. Yan, C. Liu, Y. Chen, and X.-F. Zhang, Quantum simulation of two-dimensional U(1) gauge theory in Rydberg atom arrays, [arXiv preprint arXiv:2212.10863](https://arxiv.org/abs/2212.10863) (2022).

[33] S. Sachdev, *Quantum Phase Transitions*, 2nd ed. (Cambridge University Press, 2011).

[34] T. Paiva, R. T. Scalettar, W. Zheng, R. R. P. Singh, and J. Oitmaa, Ground-state and finite-temperature signatures of quantum phase transitions in the half-filled Hubbard model on a honeycomb lattice, *Phys. Rev. B* **72**, 085123 (2005).

[35] Y. S. Elmatad, R. L. Jack, D. Chandler, and J. P. Garrahan, Finite-temperature critical point of a glass transition, *Proceedings of the National Academy of Sciences* **107**, 12793 (2010).

[36] X. Y. Xu, K. Sun, Y. Schattner, E. Berg, and Z. Y. Meng, Non-Fermi Liquid at (2 + 1)D Ferromagnetic Quantum Critical Point, *Phys. Rev. X* **7**, 031058 (2017).

[37] Y. Da Liao, H. Li, Z. Yan, H.-T. Wei, W. Li, Y. Qi, and Z. Y. Meng, Phase diagram of the quantum Ising model on a triangular lattice under external field, *Phys. Rev. B* **103**, 104416 (2021).

[38] Z.-M. Huang and S. Diehl, Interaction-induced topological phase transition at finite temperature, [arXiv:2407.04779](https://arxiv.org/abs/2407.04779).

[39] A. Ralko, M. Ferrero, F. Becca, D. Ivanov, and F. Mila, Dynamics of the quantum dimer model on the triangular lattice: Soft modes and local resonating valence-bond correlations, *Phys. Rev. B* **74**, 134301 (2006).

[40] O. F. Syljuåsen, Plaquette phase of the square-lattice quantum dimer model: Quantum Monte Carlo calculations, *Phys. Rev. B* **73**, 245105 (2006).

[41] O. Sikora, N. Shannon, F. Pollmann, K. Penc, and P. Fulde, Extended quantum $U(1)$ -liquid phase in a three-dimensional quantum dimer model, *Phys. Rev. B* **84**, 115129 (2011).

[42] Z. Yan, Y. Wu, C. Liu, O. F. Syljuasen, J. Lou, and Y. Chen, Sweeping cluster algorithm for quantum spin systems with strong geometric restrictions, *Phys. Rev. B* **99**, 165135 (2019).

[43] Z. Yan, Global scheme of sweeping cluster algorithm to sample among topological sectors, *Phys. Rev. B* **105**, 184432 (2022).

[44] The implementation of exact diagonalization analysis, finite-size scaling and data collapse through Bayesian scaling analysis in the VP-disordered phase transition, along with the estimation of the LN-VP transition boundary and the multicritical point via histograms, and the field-theoretical discussions on the finite temperature VP-Disorder transitions are presented in the Supplemental Information..

[45] H. Ballesteros, L. Fernández, V. Martín-Mayor, and A. Muñoz Sudupe, Finite size effects on measures of critical exponents in $d = 3$ $O(N)$ models, *Physics Letters B* **387**, 125 (1996).

[46] M. Hasenbusch and E. Vicari, Anisotropic perturbations in three-dimensional $O(N)$ -symmetric vector models, *Phys. Rev. B* **84**, 125136 (2011).

[47] S. M. Chester, W. Landry, J. Liu, D. Poland, D. Simmons-Duffin, N. Su, and A. Vichi, Bootstrapping Heisenberg magnets and their cubic instability, *Phys. Rev. D* **104**, 105013 (2021).

[48] M. Hasenbusch, Cubic fixed point in three dimensions: Monte Carlo simulations of the ϕ^4 model on the simple cubic lattice, *Phys. Rev. B* **107**, 024409 (2023).

[49] R. Baxter, *Exactly Solved Models in Statistical Mechanics*, Dover books on physics (Dover Publications, 2007).

[50] F. Y. Wu, The Potts model, *Rev. Mod. Phys.* **54**, 235 (1982).

[51] S. Alexander, Lattice gas transition of He on Grafoil. A continuous transition with cubic terms, *Physics Letters A* **54**, 353 (1975).

[52] Y. Q. Qin, Y.-Y. He, Y.-Z. You, Z.-Y. Lu, A. Sen, A. W. Sandvik, C. Xu, and Z. Y. Meng, Duality between the Deconfined Quantum-Critical Point and the Bosonic Topological Transition, *Phys. Rev. X* **7**, 031052 (2017).

[53] B.-B. Chen, X. Zhang, Y. Wang, K. Sun, and Z. Y. Meng, Phases of (2 + 1)D $SO(5)$ nonlinear sigma model with a topological term on a sphere: Multicritical point and disorder phase, *Phys. Rev. Lett.* **132**, 246503 (2024).

[54] J. M. Luck, Corrections to finite-size-scaling laws and convergence of transfer-matrix methods, *Phys. Rev. B* **31**, 3069 (1985).

[55] H. Shao, W. Guo, and A. W. Sandvik, Quantum criticality with two length scales, *Science* **352**, 213 (2016).

[56] X. Ran, N. Ma, and D.-X. Yao, Criticality and scaling corrections for two-dimensional Heisenberg models in

plaquette patterns with strong and weak couplings, *Phys. Rev. B* **99**, 174434 (2019).

[57] K. Harada, Bayesian inference in the scaling analysis of critical phenomena, *Phys. Rev. E* **84**, 056704 (2011).

[58] K. Harada, Kernel method for corrections to scaling, *Phys. Rev. E* **92**, 012106 (2015).

[59] K. Harada, Bayesian scaling analysis, <https://kenjiharada.github.io/BSA/>.

[60] M. Kohmoto, M. den Nijs, and L. P. Kadanoff, Hamiltonian studies of the $d = 2$ Ashkin-Teller model, *Phys. Rev. B* **24**, 5229 (1981).

[61] S. Weinberg, Gauge and global symmetries at high temperature, *Phys. Rev. D* **9**, 3357 (1974).

[62] L. Dolan and R. Jackiw, Symmetry behavior at finite temperature, *Phys. Rev. D* **9**, 3320 (1974).

[63] N. Chai, S. Chaudhuri, C. Choi, Z. Komargodski, E. Rabinovici, and M. Smolkin, Thermal Order in Conformal Theories, *Phys. Rev. D* **102**, 065014 (2020).

[64] E. Fradkin and S. H. Shenker, Phase diagrams of lattice gauge theories with Higgs fields, *Phys. Rev. D* **19**, 3682 (1979).

[65] I. S. Tupitsyn, A. Kitaev, N. V. Prokof'ev, and P. C. E. Stamp, Topological multicritical point in the phase diagram of the toric code model and three-dimensional lattice gauge Higgs model, *Phys. Rev. B* **82**, 085114 (2010).

[66] R. Nandkishore, M. A. Metlitski, and T. Senthil, Orthogonal metals: The simplest non-Fermi liquids, *Phys. Rev. B* **86**, 045128 (2012).

[67] A. M. Somoza, P. Serna, and A. Nahum, Self-Dual Criticality in Three-Dimensional \mathbb{Z}_2 Gauge Theory with Matter, *Phys. Rev. X* **11**, 041008 (2021).

[68] C. Castelnovo and C. Chamon, Entanglement and topological entropy of the toric code at finite temperature, *Phys. Rev. B* **76**, 184442 (2007).

[69] Z. Nussinov and G. Ortiz, Autocorrelations and thermal fragility of anyonic loops in topologically quantum ordered systems, *Phys. Rev. B* **77**, 064302 (2008).

[70] M. B. Hastings, Topological Order at Nonzero Temperature, *Phys. Rev. Lett.* **107**, 210501 (2011).

[71] M. Nauenberg and D. J. Scalapino, Singularities and Scaling Functions at the Potts-Model Multicritical Point, *Phys. Rev. Lett.* **44**, 837 (1980).

[72] J. L. Cardy, M. Nauenberg, and D. J. Scalapino, Scaling theory of the Potts-model multicritical point, *Phys. Rev. B* **22**, 2560 (1980).

**Supplemental Material for
"Phase transitions and remnants of fractionalization at finite temperature
in the triangular lattice quantum loop model"**

In this Supplemental Material, we first present the results of exact diagonalization for QLM on the triangular lattice in Sec. I. In Sec. II, we discuss finite-size scaling and data collapse through a Bayesian scaling analysis of the order parameters in the VP-Disorder phase transition. Thereafter, the determination of the LN-VP transition boundary and the estimation of the multicritical point are performed through an analysis of the histograms of ϕ in Sec. III. Finally, Sec. IV offers a field-theoretical discussion on the finite temperature VP-Disorder transitions.

I. EXACT DIAGONALIZATION RESULTS

In order to get some insight and to benchmark QMC results, we performed exact diagonalization on small clusters using periodic boundary conditions. On a tilted 28-site cluster (the largest cluster we could consider), there are more than 7 billion loop configurations but this number can be reduced by using various symmetries: (i) first, we can work in a given topological sector (TS), one trivial and three degenerate nontrivial ones; (ii) second, we can use all translations to reduce the Hilbert space size and also obtain the momentum; (iii) third, we can use the full point-group symmetry (here C_6 for this cluster) depending on the momentum value. Overall this allows to reduce the size to at most 66 millions configurations. We have used the Lanczos algorithm to compute the low-energy spectrum. In Fig. S1, we present our results as a function of V . For large negative V , one can clearly identify three quasi-degenerate states in the trivial TS, all at Γ momentum, as expected for the LN phase that only breaks rotation symmetry in the thermodynamic limit. Close to the RK point ($V = 1$), we observe quasi degenerate groundstates in each TS, one trivial and three degenerate in the nontrivial TSs, as expected for the QSL. In between, there is an additional low-energy state with momentum M in the trivial TS, as expected for the VP phase.

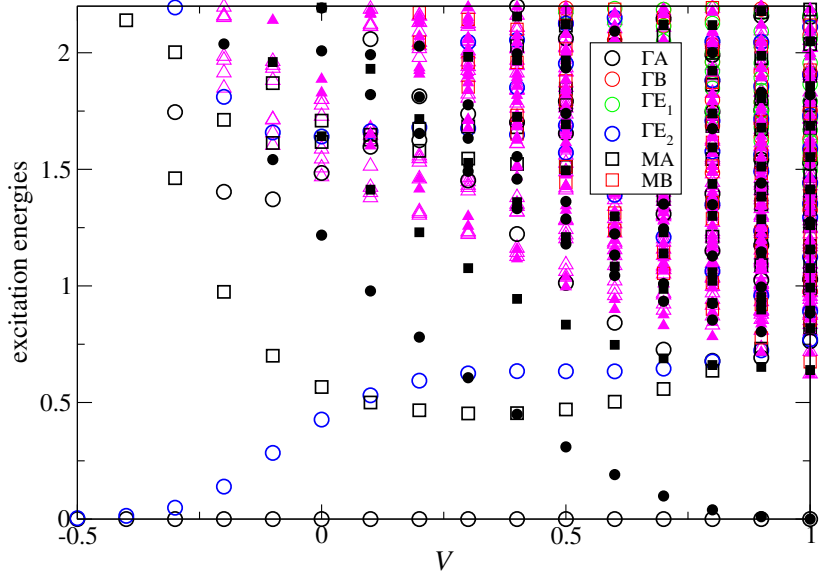


FIG. S1. Low-energy excitations versus V obtained from ED on $N = 28$ sites cluster. This cluster has C_6 point group symmetry and does contain the M point. The energy levels are labelled with their momenta, point-group symmetry as well as the topological sector (trivial/nontrivial are shown respectively with open/filled symbols). We highlight some relevant energy levels at momentum Γ (labelled using the usual C_6 irreps notations) as well as momentum M (labelled using A/B for even/odd states with respect to the reflection symmetry).

Quite importantly, we also note that the topological gap, i.e. minimum excitation energy in the nontrivial TSs, is quite large for most values of the interaction V that we have considered in the QMC simulations. This justifies that QMC simulations can be performed solely in the trivial TS to capture the universal properties of the finite-temperature LN or VP melting transitions. In particular, all the critical temperatures found in the QMC simulations are below this topological gap.

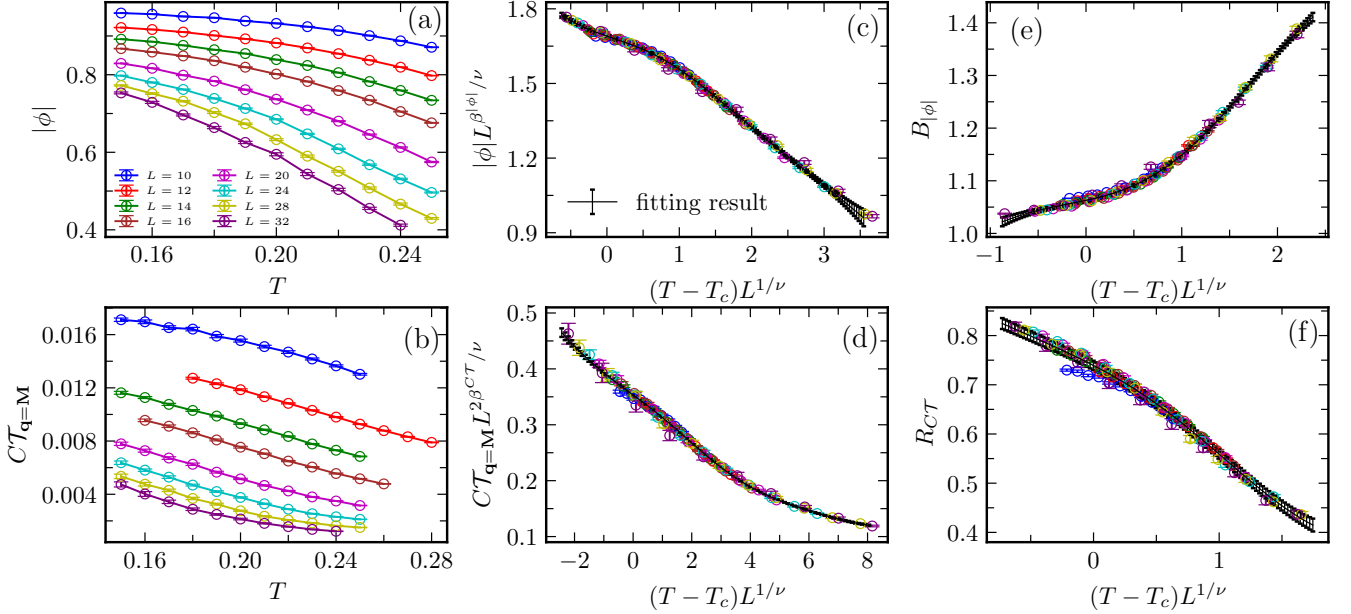


FIG. S2. Order parameters and their data collapse at $V = 0.3$. The first column displays (a) the vison order parameter $|\phi|$ and (b) the static structure factor at the M momenta of the t -term correlations $C\mathcal{T}$. The middle column shows the data collapse for these quantities using Bayesian scaling analysis in panels (c) and (d). The right column presents (e) the data collapse of the Binder ratio of $|\phi|$ and (f) the correlation ratio of $C\mathcal{T}$, with raw data provided in Fig. 3 of the main text. The fitting results for the panels (c), (d), (e), and (f) are summarized in Table I.

II. FINITE-SIZE SCALING ANALYSIS AND DATA COLLAPSE FOR THE VP-DISORDER PHASE TRANSITION

In this section, we investigate the criticality of the phase transition between the VP phase and the disordered phase using finite-size scaling and data collapse techniques. This analysis includes the determination of the transition point and aims to identify the associated universality class.

For dimensionful quantities A near the critical point, including only the leading correction term, the scaling function can be expressed as [54]

$$A(T, L) = L^{\kappa/\nu} [f^{(0)}(tL^{1/\nu}) + L^{-\omega} f^{(1)}(tL^{1/\nu})] \quad (\text{S1})$$

where $t = T - T_c$ is the reduced temperature, and ω is the correction exponent. For systems of L and $2L$, the Taylor expansion of f 's suggests that the crossing points of curves of the Binder and correlation ratios (both dimensionless quantities, that is $\kappa = 0$) as a function of T satisfy the relation [55, 56]

$$T_c(L) = T_c(\infty) + aL^{-(\omega+1/\nu)} \quad (\text{S2})$$

where a is a fitting parameter. We perform an extrapolation for the crossing points $T_c(L)$ as a function of $1/L$ for both $B_{|\phi|}$ and $R_{C\mathcal{T}}$ to determine the transition temperature in the thermodynamic limit, which is illustrated in the inset of Fig. 3 for $V = 0.3$. The extrapolation results for a few selected values of V are presented in the first column of Table I.

The data collapse for order parameters and its Binder ratio B , defined as

$$|\phi|(T, L)L^{\beta\phi/\nu} = tL^{1/\nu}, \quad (\text{S3})$$

$$C\mathcal{T}(T, L)L^{2\beta C\mathcal{T}/\nu} = tL^{1/\nu}, \quad (\text{S4})$$

$$B(T, L) = tL^{1/\nu}, \quad (\text{S5})$$

and presented in panels (b), (c), (e), and (f) of Fig. S2, are conducted using a method based on Bayesian scaling analysis, as introduced in Ref [57–59]. This approach does not require an explicit fitting form and yields superior scaling results compared to traditional least-squares methods for our data.

The fit results for three values of V within the VP phase ($V = 0.2$, $V = 0.3$ and $V = 0.4$) are summarized in Table. I. When comparing these results with the critical exponents of the two-dimensional Ising model, 4-state Potts model and related Ashkin-Teller (AT) model listed in Table. II, we first observe that our values for β^ϕ and ν lie within the range of critical exponents characteristic of the AT model. In the AT model, while the critical exponents β and ν vary along the critical line, their ratio remains fixed. However, our data yield a ratio of β^ϕ and ν of approximately 1/4, which differs from the 1/8 ratio of the AT model. Furthermore, our critical exponents derived from the data collapse differ substantially from those of the 4-state Potts model or Ising model. On the other hand, we also observe that the values of $2\beta^{CT}/\nu$ (obtained from the data collapse for CT and which corresponding to the scaling dimension of the kinetic T term) are quite large ~ 1.4 for $V = 0.2, 0.3$ and 0.4 , and close to the scaling dimension of the rank-2 symmetric traceless tensor for the (2+1) Cubic* and O(3)* transition. This seems to suggest that the observed finite temperature phase boundary of VP-Disorder transition, still experiences the influence of the ground state VP-QSL (2+1)d Cubic* QCP. It is important to note that due to the limitations in system size in our simulations, the quality of the extrapolation and data collapse are not optimal.

TABLE I. Fitting results for order parameters in the VP phase

$V = 0.2$	Extrapolation	Data collapse for $ \phi $	Data collapse for $B_{ \phi }$	Data collapse for CT	Data collapse for R_{CT}
T_c	0.17(2)	0.199(2)	0.206(2)	0.204(1)	0.219(3)
β^ϕ		0.189(6)			
β^{CT}				0.44(1)	
ν		0.79(2)	0.90(4)	0.67(2)	0.90(2)
$\omega + 1/\nu$	1.3(1)				
$V = 0.3$					
T_c	0.16(1)	0.161(4)	0.168(2)	0.177(1)	0.181(2)
β^ϕ		0.22(2)			
β^{CT}				0.528(7)	
ν		0.91(4)	1.01(4)	0.741(8)	0.98(2)
$\omega + 1/\nu$	1.5(1)				
$V = 0.4$					
T_c	0.13(2)	0.135(2)	0.142(2)	0.138(1)	0.150(2)
β^ϕ		0.212(8)			
β^{CT}				0.45(2)	
ν		0.77(3)	0.82(4)	0.63(2)	0.68(1)
$\omega + 1/\nu$	1.4(2)				

TABLE II. Critical exponents for two-dimentional Ashkin-Teller (AT) models on the critical line, 4-state Potts model, and Ising model [49, 60]

	β	ν	β/ν
AT	$[\frac{1}{12}, \frac{1}{4}]$	$[\frac{2}{3}, 2]$	$\frac{1}{8}$
4-state Potts	$\frac{1}{12}$	$\frac{2}{3}$	$\frac{1}{8}$
Ising	$\frac{1}{8}$	1	$\frac{1}{8}$

III. ORDER PARAMETER AND HISTOGRAM IN THE LN-VP PHASE TRANSITION

In this section, we present supplementary data regarding the first-order transition between the LN and VP phases, as indicated by the square marker in the overall phase diagram shown in Fig. 1. The order parameters $\langle D \rangle$ and $|\phi|$ as a function of V at $T = 0.1$ for various system sizes are displayed in Fig. S3. The clear change of the finite size dependence around $V \sim 0$, indicates that $\langle D \rangle$ and $|\phi|$ behave differently in the LN and VP phases.

To determine the nature of the phase transition, we consider the histograms of the vison order parameter ϕ , as shown in Fig. S4. We first focus on $T = 0.1$ (first row in Fig. S4, corresponding to the lower gray dashed line in Fig. 1) as an example. We observe a transition in the histogram peaks from a face-centered cubic structure to a

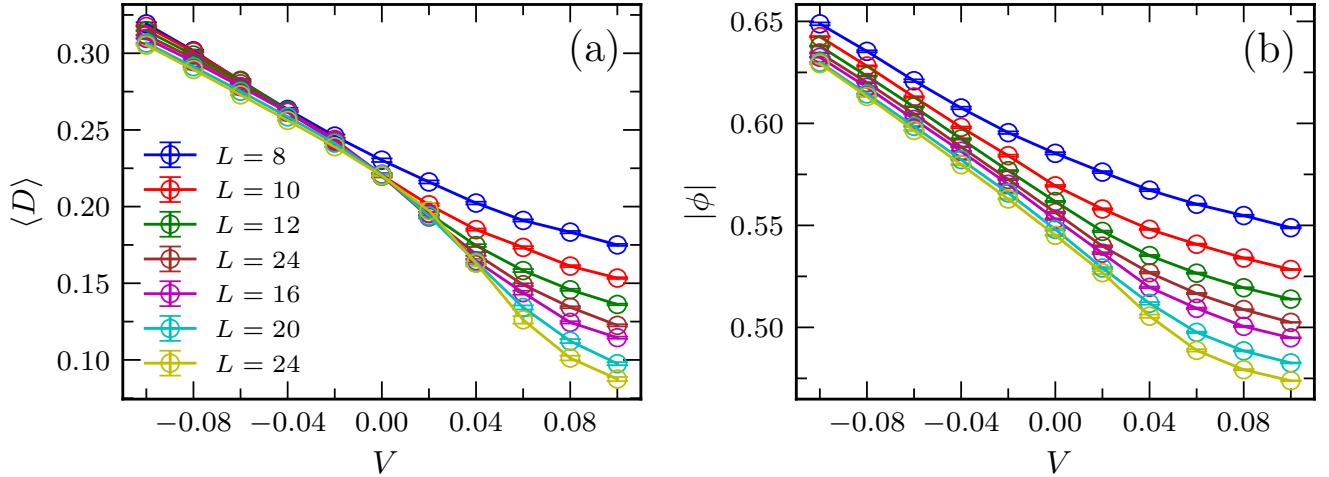


FIG. S3. Order parameters (a) $\langle D \rangle$ and (b) $|\phi|$ as a function of V at $T = 0.1$ for various system sizes. The clear change of the finite size dependence around $V \sim 0$, indicate that $\langle D \rangle$ and $|\phi|$ behave differently in the LN and VP phases.

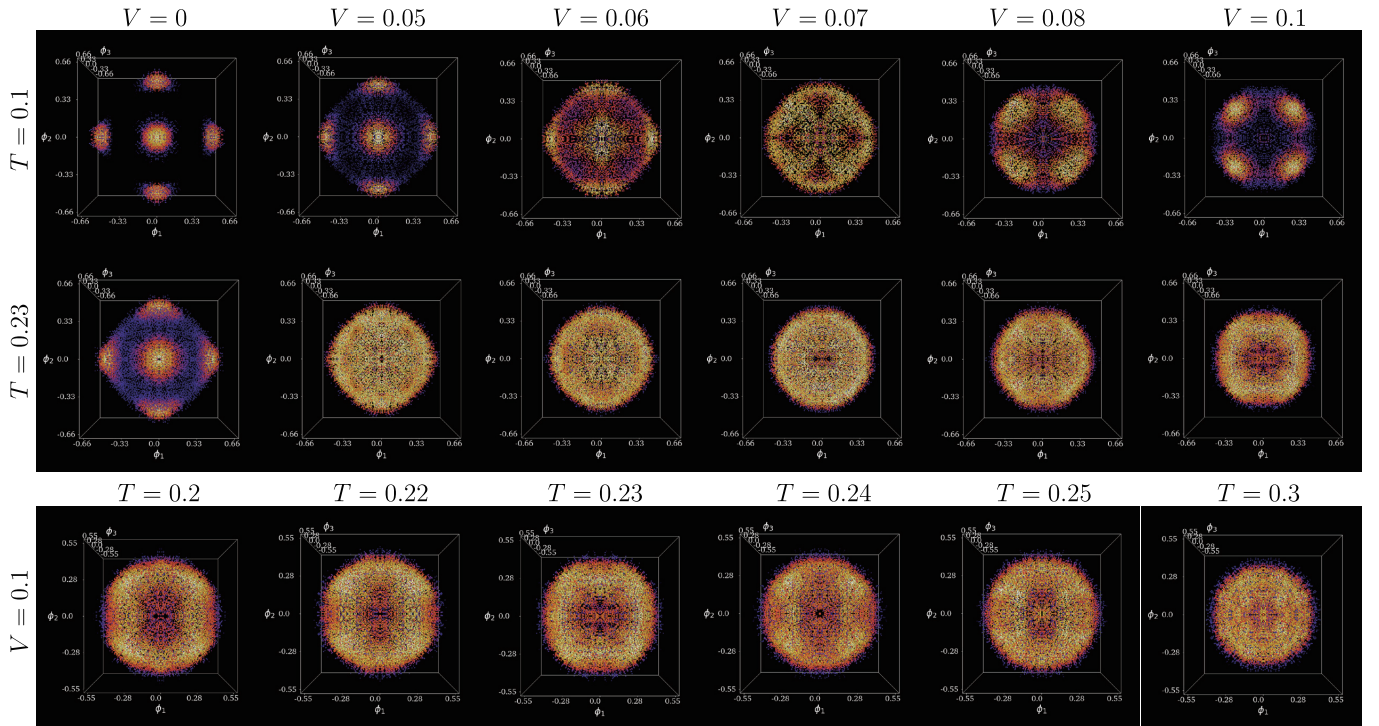


FIG. S4. Histograms of the veson order parameter ϕ . The first row, corresponding to $T = 0.1$, illustrates the changes in the histogram associated with the first-order transition between the LN phase and the VP phase at finite temperature. This transition features a change from a face-centered cubic anisotropy to a corner-cubic anisotropy for the histogram peaks. The transition point is identified at $V = 0.07(2)$ for this temperature. The second row depicts the histogram at $T = 0.23$, the LN order appears to melt directly into the disordered phase, with a transition again close to $V = 0.07(2)$. These data serve as a supplement to the right column of the Fig. 4 in the main text. In the third row of the figure, with V fixed at 0.1, the VP phase disappears as the temperature increases. Based on such results and those with finer temperature and V scans (not shown), we estimate the location of the multicritical point around $(V, T) = (0.07(2), 0.22(2))$ (marked by the red star in Fig. 1).

corner-cubic structure, with a coexistence of both at the transition point at $V = 0.07(2)$ suggesting a first order phase transition. This analysis can also be applied to identify transition points at other temperatures. In the second row of Fig. S4, which displays the histogram at $T = 0.23$ (marked by the upper gray dashed line in Fig. 1), the LN order appears to melt directly into the disordered phase, with a transition again close to $V = 0.07(2)$. The third row of Fig. S4 illustrates the disappearance of the VP order at a fixed value of $V = 0.1$ as the temperature increases. This disappearance begins at $T = 0.23$, suggesting that the VP phase transitions directly to a disordered phase for this value of V .

IV. THEORETICAL EXPECTATIONS FOR THE FINITE TEMPERATURE VP-DISORDER TRANSITION

In this section, we analyse the behaviour of the theory Eq. (2) at finite temperature. We work in $4 - \epsilon$ dimensions to study its fixed point and the finite temperature phase diagram. For simplicity, let us work with a single scalar first

$$S = \int d\tau d^d x \mathcal{L}, \quad \text{with} \quad \mathcal{L} = \frac{1}{2} \partial_\mu \phi \partial^\mu \phi + \frac{1}{2} \phi^2 + \frac{1}{4!} \lambda \phi^4 \quad (\text{S6})$$

One can expand the scalar theory using Fourier/Matsubara modes along the temporal circle

$$\phi(x, \tau) = \phi_0(x) + \sum_{2n \in \mathbb{N}} \phi_n(x) e^{\frac{2\pi n}{\beta} \tau} + \phi_n^\dagger(x) e^{-\frac{2\pi n}{\beta} \tau}. \quad (\text{S7})$$

The temporal circle has radius $\frac{\beta}{2\pi}$. Notice that due to the Z_2 gauge symmetry, the scalar can take both periodic and anti-periodic boundary conditions. The index n for the Matsubara modes can be half integer. After the Fourier expansion, we get

$$S = \int d^d x \mathcal{L} \quad (\text{S8})$$

with

$$\mathcal{L} = \frac{1}{2} \partial_\mu \phi_0 \partial^\mu \phi_0 + \sum_{2n \in \mathbb{N}} \partial_\mu \phi_n \partial^\mu \phi_n^\dagger + \sum_{2n \in \mathbb{N}} \frac{4\pi^2 n^2}{\beta^2} \phi_n \phi_n^\dagger + \frac{\lambda}{2} \phi_0^2 \sum_{2n \in \mathbb{N}} \phi_n \phi_n^\dagger + \frac{\lambda}{4!} \phi_0^4. \quad (\text{S9})$$

The theory is a massless scalar interacting with infinitely many massive scalars. The one loop diagram with massive loop will renormalize the mass of the zero mode, we get

$$m_{\text{th}}^2 = \sum_{2n \in \mathbb{N}} \frac{\lambda}{\beta} \int \frac{d^3 k}{(2\pi)^3} \frac{1}{k^2 + (\frac{2\pi n}{\beta})^2} = -\frac{\lambda}{2\beta^2} \sum_{2n \in \mathbb{N}} n = -\frac{\lambda}{4\beta^2} \zeta(-1) = \frac{\lambda}{48} \beta^{-2}. \quad (\text{S10})$$

The works of [61, 62] studied scalar theories without the Z_2 gauge symmetry, and obtained $m_{\text{th}}^2 = \frac{\lambda}{24} \beta^{-2}$. The Z_2 gauge symmetry reduces the size of the thermal mass by a factor 2. Working in $4 - \epsilon$ dimension, we find that the beta function of the λ coupling takes the form

$$\beta_\lambda = -\epsilon \lambda + \frac{3}{16\pi^2} \lambda^2. \quad (\text{S11})$$

The fixed point at $\lambda = 16\pi^2 \epsilon / 3$ is the critical Ising model. Substituting the critical coupling λ into the thermal mass [63], we get

$$m_{\text{th}}^2 = \frac{\pi^2 \epsilon}{9} \beta^{-2}.$$

At $\epsilon = 1$, that is $D = 2 + 1$ dimensions, the above formula will be modified. A simple dimensional analysis, however, tells us that

$$m_{\text{thermal}}^2 = c T^{1/\nu}, \quad (\text{S12})$$

where c is a dimensionless constant. The finite temperature occurs when $m_{\text{thermal}}^2 + m^2 = 0$. Near the quantum critical point, $m^2 \sim -|V - V_c|$. Together they lead to

$$T_c \sim |V - V_c|^\nu. \quad (\text{S13})$$

Even though we have used the critical Ising model as an example, the above discussion can be applied to other conformal field theories (CFT), such as the Cubic* fixed point in Eq. (2). The above discussion suffers from a significant subtlety. Applying it to the Ising* transition [64–67] from the toric code phase to the trivial phase, one would conclude that the phase transition survives at finite temperature. It is, however, well-known that there is rather a cross-over instead of a true phase transition, since the toric code phase does not persist at finite temperature [68–70]. The toric code phase has massive anyons, including the e and m particles, the thermal fluctuation of these particles will destroy the topological order. For our loop model, the local constraint completely forbids the creation of free electrically charged particles, the spinons [3]. The above discussion focusing solely on the magnetically charged degrees of freedom, the visons ϕ_i in Eq.(2), therefore makes sense.

We now discuss what could be the critical behavior of Eq. (2) when put at finite T . We expect a scalar theory respecting the Cubic symmetry in two spatial dimensions.

One candidate theory that may describe the corresponding VP-Disorder transition is three decoupled copies of Ising models, based on the following reasoning. Let us denote the spin operator and the energy operator of the three Ising copies as σ_i and ϵ_i . The CFT preserves the three Z_2 symmetries that flip the signs of σ_i as well as the permutation symmetry S_3 which permutes the three decoupled Ising copies. Notice the Cubic group is isomorphic to $S_3 \ltimes (Z_2)^3$. The phase transition is triggered by a coupling sO with $O = \epsilon_1 + \epsilon_2 + \epsilon_3$: when $s > 0$, the system is in a disordered phase and when $s < 0$, the three σ_i 's get expectation values (vev) which can be positive or negative, leading to eight corner-cubic states corresponding to the VP phase. Near the QCP, we thus expect a VP-Disorder critical behavior in the (decoupled) Ising universality class.

Away from the quantum critical point, however, another candidate is the 4-state Potts universality class. The gauge invariant order parameter for the VP phase is given by the kinetic t_i -terms, which correspond to scalar bilinear fields $t_1 = \phi_1\phi_2, t_2 = \phi_2\phi_3, t_3 = -\phi_1\phi_3$ [28, 29]. The operators $\{\phi_1\phi_2, \phi_2\phi_3, -\phi_1\phi_3\}$ form a irreducible triplet representation of the Cubic group. It is, however, not a faithful representation. The subgroup faithfully represented on the triplet is the permutation group S_4 , as hinted by the tetrahedron shapes in Fig. 3 (c) and (f) when $\phi_i = \pm \text{vev}$. The breaking of the S_4 symmetry may thus lead to the 4-state Potts universality class. We note that both CFTs have exact marginal operators. This is well known for the 4-state Potts model [71, 72]. For the decoupled Ising universality class, the exact marginal operator is $O_2 = \epsilon_1\epsilon_2 + \epsilon_2\epsilon_1 + \epsilon_1\epsilon_3$ which has scaling dimension 2 due to $\Delta_\epsilon = 1$ for the Ising CFT. The logarithm corrections induced by these marginal operators may obscure finite-size scaling.
